Available online at www.sciencedirect.com

jmr&t Journal of Materials Research and Technology

journal homepage: www.elsevier.com/locate/jmrt

Original Article

Cellular automaton-based simulation of bulk stacking and recovery

Matheus Henrique de Castro, José Aurélio Medeiros da Luz, Felipe de Orquiza Milhomem*

Mining Engineering Department, School of Mines at Federal University of Ouro Preto, Ouro Preto, MG, 35400-000, Brazil

ARTICLE INFO

Article history:
Received 12 July 2021
Accepted 24 November 2021
Available online 4 December 2021

Keywords:
Granular material
Stockpile
Granular flow
Cellular automata
Modeling

ABSTRACT

Stockpiling is a key issue in bulk material handling. A small-scale, quasi-two-dimensional physical model was used to investigate size segregation during stacking and gravitational reclaim of stockpiles and to compare experimental results to those ones generated by a simplified mathematical model. This mathematical model is based on cellular automata and was used to simulate size segregation in conical stockpiles of non-cohesive granular material and gravity flow during its reclaim, through a ground level discharge opening. The present model has taken into account only three particle size class. Banded layers of fine, medium-sized, and coarse particles appear during the pile growth. These stratification patterns have been observed during stockpile formation both in the physical model and in the cellular automaton-based model. Also, experiments in both physical and cellular automaton-based model were carried out to quantify the particle size time evolution of granular material leaving the discharge opening during reclaim. Furthermore, the cellular automaton-based model has successfully simulated segregation phenomena during gravitational discharging, as well as the topological features of segregation during stockpiling and reclaim.

© 2021 The Authors. Published by Elsevier B.V. This is an open access article under the CC BY-NC-ND license (http://creativecommons.org/licenses/by-nc-nd/4.0/).

1. Introduction

Granular materials are abundant in nature. There are examples of such systems in the beach sand, in the desert dunes and even in the ice grains that make up the Saturn's rings. Granular materials account for about 75% of all raw materials in stock and are the second most handled material in the industry, with water being the first one. Granular material handling is always present in mining and metallurgical sectors, mainly in the stacking and reclaim of ore storage and homogenization stockpiles, as well as in hauling by conveyor belts.

Granular materials generally tend to segregate when subjected to external disturbance. The mechanisms that take part in this phenomenon are multiple, such as: London-van der Waals forces, differences in density, shape, and grain size. The last case is the so-called particle-size segregation.

* Corresponding author.
E-mail address: jaurelio@ufop.edu.br (J.A.M. da Luz).
https://doi.org/10.1016/j.jmrt.2021.11.127
2238-7854/© 2021 The Authors. Published by Elsevier B.V. This is an open access article under the CC BY-NC-ND license (http://creativecommons.org/licenses/by-nc-nd/4.0/).

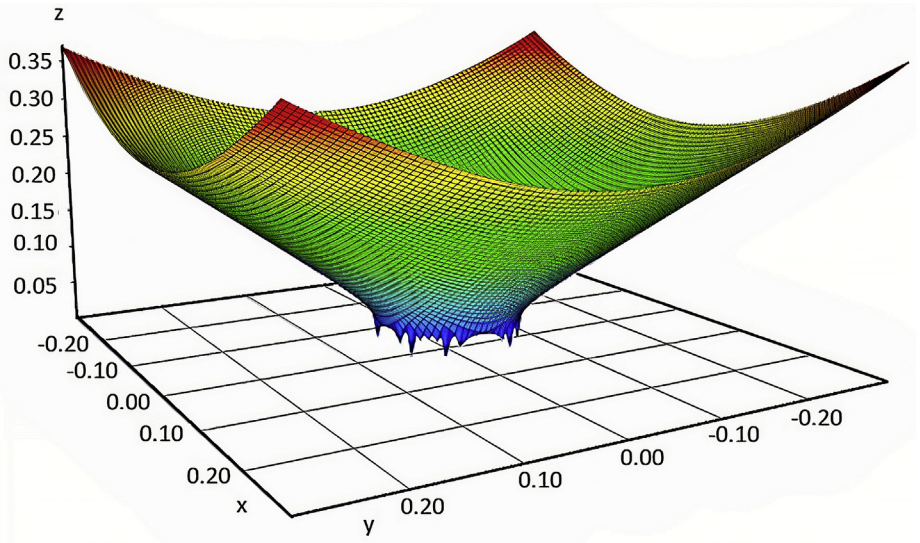

Fig. 1 – A funicular reclaim surface with circular cross-section outlet whose center falls in (x, y, z) ≡ (0, 0, 0).

The densified and non-cohesive granular media have an overly complex behavior, sometimes being able to behave as either solids or liquids, and an intermediate behavior between these two extreme limits is common. When the movement begins, one can observe a common increase in fluidity for finer particle systems [1,2]. Romanowski, Grudzien, and Williams [3] have studied the application of electrical capacitance tomography, exploring the behavior of bulk material flow during hopper discharge including spatial modelling using homogenous Markov random field images for detection of hopper flow instabilities. In turn, Larsson et al. [4] have used digital speckle photography, aiming at characterizing the granular system flowability and have concluded this technique ensures high accuracy in the analysis of granular flow behavior. Tucci et al. [5] have employed unmanned aerial vehicle-based photogrammetry to inspect and evaluate stockpiles of bulk material, and they achieved great accuracy for the case studied.

Despite of employing the quite theoretical approach of cellular automaton-based simulation, this work falls within the field of mathematical modelling of real-world problems in engineering, industrial and environmental systems. Silos, bins, hoppers and stockpiles are widely used for bulk solids handling and storage in the industrial sector. Usually, industrial granular stockpile is conical or prismatic (with a triangular cross-section), either with a straight axis or a kidney-shaped one. Sometimes it is built up by superposition of cones or strings, depending on its construction method and its shape [6,7].

A simple method of constructing stacks is made by stacking material from fixed height. The continuous granular material accumulation around this feed axis recurrently exceeds the stability of the system, resulting in avalanches, which redistribute the mass from the top of the stack to its base, generating a conical surface characterized by the material's angle of repose. The angle of repose is indicative of the fluidity and cohesion of a granular system, and can be used in different fields, such as agriculture, pharmacology, geology, mining, bulk handling, among others [8]. Several factors can affect the angle of repose, such as particle size and shape, rolling friction coefficient, moisture, Archimedean thrust, London–van der Waals interactions, among others. So, this dynamic behavior is complex and linked to the aperiodic phenomenon of self-organized criticality.

The kinetic energy gain as the particle drops or falls, and its dissipation during stacking, acts on different scales for each grain size. Finer particles have lower potential energy and therefore get lower kinetic energy gain. When they collide inelastically against coarser particles, they lose their small impulse, and often they end up caught between the interstices of coarser particles. Falling coarser particles, on the other hand, have higher potential energy gaining more kinetic energy, and when they interact by friction and collisions with finer particles, they find less resistance or barriers to their movement, more frequently reaching the base of this heterogeneous pile, because a surface made up of tiny particles is relatively less "corrugated" for a coarse particle in sliding movement. In this line, Benito, Ippolito, and Vidales [9], studying quasi 2D piles, have showed the increase of the dumping point height leads to greater size segregation, due to the final higher kinetic energy. In turn, Rodríguez et al. [10] studied the segregation of quasi 2D piles using glass beads and coriander seeds. According to their results, layering, blending or segregation may alternatively occur, depending on roughness, size, and density of the particles.

Particle-size segregation is deleterious to industrial handling because processes do require adequate feeding homogeneity. Finished product stockpiles may have an even narrower range for material variability to meet quality standards. Thus, the operational techniques for stockpile reclaim must have rules and criteria depending on the construction history of the pile itself. According to Larcher and Jenkins [11], the flow rheology is strongly impacted by size segregation, with the difference in particle sizes more strongly influencing the segregation than the weight of the solid. Liao and co-

workers [12], in turn, have studied the addition of small amounts of water to granular medium in a rotary drum and have found there was a decrease in segregation.

Just to cite an instance, also a very widespread concept exists for gravity flow of granular materials in underground mining (particularly under the sublevel caving method). The approach by Janelid and Kvapil [13] defines a flow ellipsoid as an envelope of the granular material's stream tube. The initial flow of material between two exploitation galleries will come from an ellipsoidal region starting from the discharge opening, its upper limit being the surface of the broken material. The material that is located outside this initial ellipsoid and inside a boundary ellipsoid will have some displacement and mobility but will not reach the discharge at the first stage of reclaim. Following the initial discharge, a reclaim hyperboloid arises from the subsidence of the broken material surface, and this curve indicates the regions where there will be the greatest grain displacement. On the other hand, fragments outside the boundary ellipsoid will not undergo any displacement and, therefore, will not reach the discharge [14]. Of course, in two-dimensional systems the ellipsoids degenerate into ellipses.

Regarding stockpiling, the present authors have been studying the prediction of live volume fraction for a conical pile reclaimed through a ground level outlet opening. Mathematical modeling has been carried out and it will be object of future papers. In brief, the funicular revolution curve around the z-axis can be described as a function of the equivalent radius (r) of the discharge hole, the pile diameter (D), the static and dynamic angles of repose (β and α, respectively). This kind of function can fit for reclaiming crater with rat-hole occurrence and it is expressed by the following expression:

$$z = f\left(\sqrt{x^2+y^2}\right) = \left[\left(\frac{\sqrt{x^2+y^2}}{r}\right)^6 - \left(\frac{\sqrt{x^2+y^2}}{r}\right)^2\right]^{\frac{1}{6}} \times r \times tg(\beta) \quad (1)$$

Here, β is the angle of static friction or angle of reclaim, of a flat slope (an asymptotical value). In Fig. 1, $r = 0.007$ m and $\beta = \alpha + 3 = 41.2°$.

Anyway, the great complexity of the gravity flow of a granular system, with its constitutive equations very difficult to obtain, makes attractive the idea of using simpler descriptive tools to describe it, even if they are of a more abstract nature. In this line, an approach with great potential is to employ the so-called cellular automata (CA). Ultimately, this pivotal point is the research gap behind this study.

Cellular automata are discrete computational systems and have been increasingly used to simulate complex systems and have been employed to simulate the dynamical aspects, and evolution of non-linear systems, as crystal growth, urban evolution, and progression of disease, for instance.

Cellular automata (CA) are mathematical models used in the study of a wide variety of systems characterized by local interactions. Applications cover areas of physics, chemistry, and biology, among others. Examples of studies carried out with the use of cellular automata are urban traffic modeling [15–17], seismicity modeling (Xanthi, in Northeastern Greece) [18], material corrosion [19], flow in porous media [20], simulate grain growth evolution in material sciences [21–23], prediction of disease spreading [24–26], like HIV, hepatitis or Covid-19 [27–29], among others. A cellular automaton can be defined as a set of discrete variables arranged on nodes of a network in a discrete space, subject to specific rules for its movement.

The time evolution of an automaton occurs through some imposed dynamic rules, which act on each network variable, considering only the first neighborhood of the node in which this variable actually is located. The rules can be local probabilistic or deterministic in nature. All network nodes are updated simultaneously, and each synchronous update performed corresponds to a time step. Thus, time is also defined in a discrete way. For instance, as granular material is concerned, Alonso, Hovi and Herrmann [30] have achieved a cellular automaton-based method for forecast angle of repose of piles using devil's staircase concept.

Physical models have a well-defined field of use over the last sixty years in various areas of knowledge. Experiments in small scale models are useful in the characterization of the problem and can indicate project criteria and forecast industrial performance [31].

Fan et al. [32] have gathered a historical series of data from other investigators' experiments, in order to investigate the segregation phenomenon during pile formation. Grasselli and Herrmann [33] have evaluated the effects of wall separation and flow rate on stratification patterns and found out that the layered pattern depends strongly on the mass flow rate feeding the pile. The wavelength (or the characteristic distance between successive layers) increases with the mass flow rate and decreases with the wall separation (span). These two variables are interconnected according to energy dissipation during the pile erection operation.

Following this line of thought, experiments in a quasi-two-dimensional physical model were used in the present work, for validation of the cellular automaton-based model, more specifically in regard of gravity granular flow.

2. Objective

The aim of this study was to model the erection of stockpiles and their gravitational recovery (reclaim through a ground level opening) by cellular automata based on deterministic and probabilistic rules, from a two-dimensional approach.

3. Materials and methods

3.1. *Small-scale model and samples*

The walls of the physical model were two parallel glass plates 70.0 cm wide by 35.0 cm high, being spaced by 1 cm thick wooden slats, configuring a quasi-two-dimensional bin (or stockpile), aiming at validating the computational model.

A top feeding hole (connected to a mass flow funnel hopper) and a basal opening (outlet slot) were disposed axisymmetrically. The outlet slot dimensions are: length of 3.0 cm and width of 1.0 cm. The built discharge aperture represents a ratio of outlet to pile's bottom ("diameter") equal to 0.05.

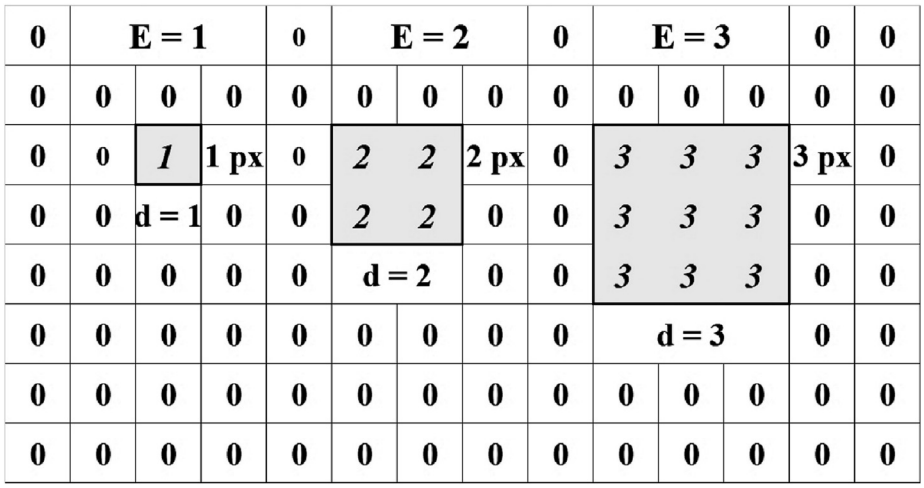

Fig. 2 – Sizes of different particles in CA model.

The output results of the model are the observed segregation and stratification patterns and the variability of then granular material draw from the pile, as well as the variability of the granular material after successive feedings in the live volume of the pile.

Bulk material samples were prepared in only three quasi-monodisperse grain sizes of the same density, in order to minimize the variables involved in the experiments. Colored quartz sand was employed. The fine size class material (milky color) was graded in range between the 300 μm and 212 μm; the intermediate material (purple) in the range between 600 μm and 500 μm, whereas the coarse material (orange color) in the range between 1120 μm and 850 μm. The fine sand angle of repose was found to be 32.5°. The angle of repose was 37.4° for the medium sand, while the coarse sand has resulted in 38.2° for that parameter. Concerning the present model dimensions, the typical width of the pile bottom is around 60 cm for 1.200 kg of bulk material.

The sampling of the reclaimed material at pile's discharge was carried out by a compartmented sampling box located under the pile opening, which could travel orthogonally to the pile's glass walls. Once each compartment (drawer) of the sampling box was filled up, the granular flow was interrupted as a consequence. Subsequently the next compartment was pushed manually underneath the outlet slot. In effect, at the beginning of the pile building up process, the discharge slot was already open, so the first sample (that filled the first compartment up) represented the feeding material blend. The stockpile feed was homogenized carefully and dropped from a small mass-flow conical bin, in order to avoid its size segregation.

A few words about simplifying the system for the two-dimensional case should be stated here. Although the simulation in this work was carried out bidimensionally, in granular systems of low cohesiveness — with axisymmetric geometric conformation, such as a cone — its extrapolation to three-dimensional systems can be made using the second Pappus–Guldinus theorem (centroid theorem), since it is a solid of revolution, without appreciable errors. This theorem is very intuitive and states that the volume of a solid of revolution is the product of the area of the rotating plane figure and the path traveled by its centroid, during the movement around the axis of rotation.

However, in those granular systems where there is ponderable interparticle interaction, simple integration to 3D systems requires correction factors, resulting from the confinement effect, especially where there are small radii of curvature of the pile surface (near the discharge opening, at the end of reclaiming cycle), embodied by the so-called cohesive arch formation. This treatment is beyond the scope of this study and will be subject of a future publication.

Furthermore, the comparison of the spatial heterogeneity within the conical stockpile (with its granulodensimetric segregation pattern) is fully justified by the comparison with the quasi-two-dimensional experimental pile employed. For the actual case of three-dimensional cohesive systems, much more sophisticated techniques, such as the use of deep-penetration X-ray tomography (or even high-resolution electrical resistivity tomography), would be required to compare the spatial heterogeneity, counterproductively increasing the complexity and cost of the experimental campaign.

3.2. *Cellular automata (CA) modeling*

The cellular automaton-based model used an array of 600 rows per 1200 columns for the two-dimensional cell representation. Its mathematical features are discussed below.

3.2.1. *Particle size distribution and stockpile composition*

The smallest discrete size of a CA mesh is the equivalent of a unit cell, or even a pixel. The state of a cell can be occupied by the integer values $E = \{0, 1, 2, 3\}$. To represent an empty space the value 0 will be assigned to the cell, and the state $E = 1$ represents a grain of class P_1 with a diameter equal to 1 (strictly, an edge equal to 1 pixel or 1 unit cell). Larger grains are represented by more than one unit cell, such as clusters. Therefore, four cells ($4 = 2 \times 2$) with state $E = 2$ represent a grain of class P_2 equal to 2 in diameter (strictly, edge width of 2 pixels, or 2 contiguous unit cells), and nine cells with state $E = 3$, represent a grain of class P_3 of diameter equal to 3

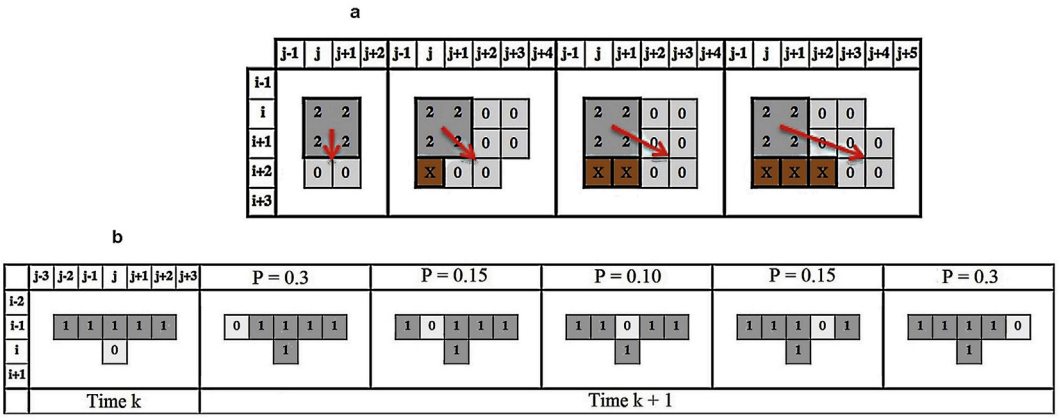

Fig. 3 — Neighborhood conditions for particle motion and first probability rule for gravitational flow. 3a — Neighborhood conditions for particle motion (cells labeled with X represent other particles of class 1, 2 or 3); 3b — First probability rule for gravitational flow concerning a particle of class P1 (uppercase P in the first line is the probability of occurrence).

(strictly, with an edge equal to 3 pixels, or 3 contiguous unit cells). By adoption, these classes have only two degrees of freedom, and can move only horizontally and vertically downwards, without exhibiting any deformation or fragmentation (Fig. 2).

Particle density does not have much influence in stratification phenomena, unless in case of great density discrepancy. The inclusion of this physical quantity in the CA model implies the inclusion of additional parameters related to potential energy and inertia for each particle. Thus, the present model has adopted the density as invariant, that is, equal densities are assumed for any grain size. Consequently, the mass fraction $F_{m,i}$ of each size becomes equivalent to the area occupied by the particle i in the 2D mathematical model.

3.3. *Formation and reclaim of stockpile*

The width of the feeding stream was adopted equal to 2% of the stockpile width (equivalent to 24 columns), whereas the discharge opening was 5% of the stockpile width (equivalent to 60 columns).

To simulate the stockpile stacking process (formation), successively particles were added in the upper position of the stockpile's axis of symmetry, while particles are drawn (removed) from the built-up stockpile in the bottom position of the stockpile's axis of symmetry, in order to simulate the reclaim. Both cell feeding and reclaiming in the model were made from the stochastic drawing of an abscissa j (an array's column), according to a truncated Gaussian distribution with mean in $j = 600$, that is, in the axis of symmetry of the array. The truncation was done by limiting the realizations within the range of $[-3\sigma, +3\sigma]$. In case of stacking, the standard deviation (σ) was adopted equal to 1/6 of the width of the feeding jet. On the other hand, in case of reclaim simulation, the standard deviation (σ) was adopted equal to 1/6 of the width of the discharge opening, making the mathematical model compatible with the dimensional parameters of the corresponding physical model.

The algorithm used to generate realizations according to the normalized Gaussian distribution was the classical computational routine from Box-Müller [34]. Each draw employs two pseudorandom variables ($0 = U_1 \leq 1$, and $0 = U_2 \leq 1$) and generates two normalized Gaussian realizations (ξ_1 and ξ_2 with mean zero and unit variance), according to Equations (2) and (3):

$$\xi_1 = \cos(2\pi \times U_1) \times \sqrt{-2 \times \ln(U_2)} \quad (2)$$

$$\xi_2 = \sin(2\pi \times U_1) \times \sqrt{-2 \times \ln(U_2)} \quad (3)$$

3.3.1. *Migration rules for bulk material particles stacking simulation*

Motion directions of the particles in the model are only descending (downward) or side displacements. The final position of the particle depends only on the presence of an immediately lower stable surface, wide enough that there is no collapse (micro-avalanche/overturning). Thus, the algorithm first checks if there is a vertical free path below the particle. Secondly, it checks whether there is a free path toward the left or the right side of the particle. Afterwards, the extension of the surface on which the particle is seated is checked, prioritizing the more vertical movements or the shorter distances (Fig. 3a).

In order to simulate angles of repose, a particle was submitted to two rules. The first one was deterministic and the second one stochastic, having a probability of occurring, even if it there was a free path, thus obtaining a devil's staircase on the pile surface.

3.4. *Migration rules for bulk material particles in reclaim simulation*

In this model, gravity flow will occur in a probabilistic way, with neighborhoods similar to those used in hopper flow simulation by Kozicki and Tejchman [35] using cellular automata. The most practical case is when the cell (i, j) represents an empty space and has the upper 5 neighboring cells occupied by particles of class P_1. Larger probabilities were set

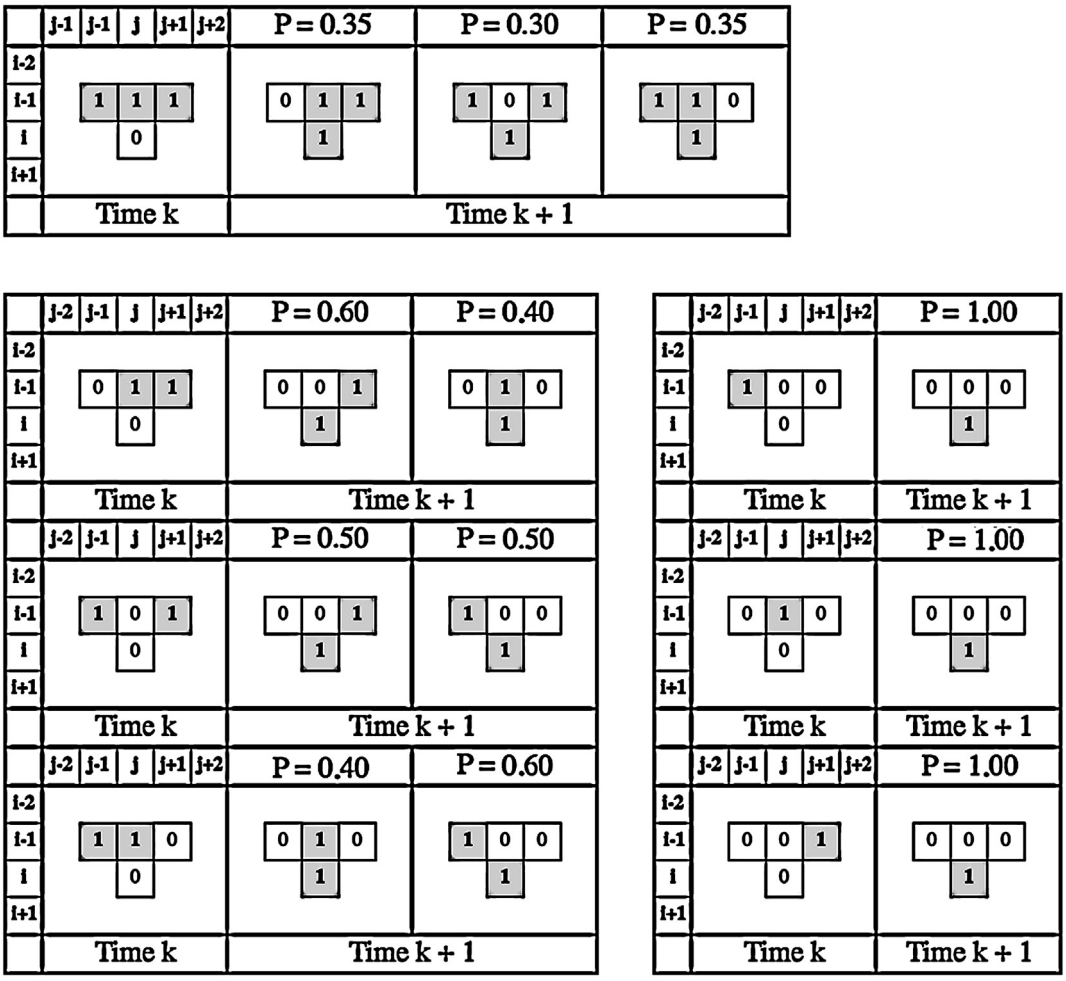

Fig. 4 – Second probability rule for gravitational flow concerning a particle of class P_1 (uppercase P in the first line is the probability of occurrence).

for the side particles to occupy the empty space below (Fig. 3b). Although this argument is counterintuitive, the overall result of the flow behaves in the correct way, since all empty cells during the reclaim appear in the vicinity of the axis of symmetry of the outlet opening. The probabilities of a single grain moving leftward or rightward can null each out. In the macro scale, as the empty spaces moves upwards, reaching the stockpile surface in different regions, the final surface of subsidence resembles a pattern similar to a crater (with upward concavity), symmetric with respect to the discharge opening.

Other conditions emerge and need to be considered in sequence. In order to reduce the number of hypotheses tested (which are potentially many), if the first flow rule is not a match, the second rule is to check if the three upper neighboring cells are occupied by particles of class P_1 (Fig. 4). If this is not the case, it is tested the hypothesis of an already existing empty space in the row just above the targeted cell.

Regarding the problem due to the heterogeneity of grain size, the rules mentioned so far alone will result in the gathering of empty cells underneath the larger particles, allowing them to only move downwards. To make room for the larger particles to move downwards and sideways, there is a specific rule to allow the particles of class P_1 that are located in the bottom sides of the larger particles. This rule in small scales results on a resemblance to the arching effect (Fig. 5).

Then the next rules look out for sets of empty spaces and then check for the presence of the coarser particles. The priority here is firstly to check for the most vertical motion possible, verifying initially the occurrence of symmetry. If symmetry is not found, then the individual motion for the occasional particle is tested, on the left side or the right side in order to fill in the empty cells below. This is summarized in Fig. 6.

The mathematical model based on cellular automata was implemented in Free Pascal, using Lazarus, a free open-source platform with integrated development environment.

3.5. *Measuring similarity between mathematical and physical models*

A simplified method was developed to quantify, even if in an expeditious way, the similarity degree between the experimentally constructed stockpiles in quasi two-dimensional bin

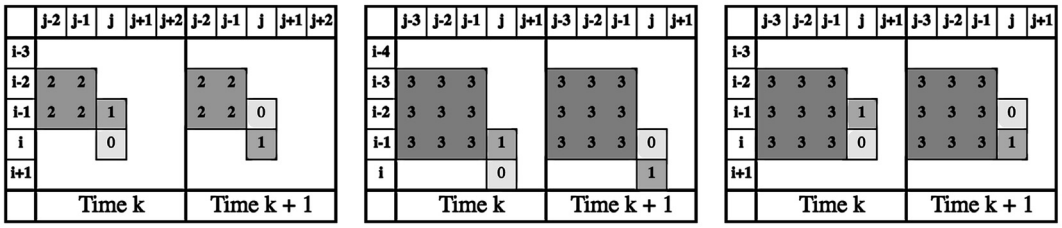

Fig. 5 – Probability rule for gravitational flow concerning particles of class P_1, P_2, and P_3 (uppercase P in the first line is the probability of occurrence).

and those corresponding to the cellular automaton-based simulation, discussed here. Strictly speaking, an analysis like that based on geostatistical methods (dealing with regionalized variables) would be necessary in order to characterize the inner structure of the chromatic value transitions of the pixels, which are linked to the size segregation of the granular material in stockpile. Alternatively, a fractal approach also would be promising in revealing the above-mentioned pile's inner structure.

To perform the simplified similarity measurements, firstly the experimental and simulated images of the piles were transformed into grayscale images (in *jpg* format). In order to select the more conspicuous segregation pattern, it was decided to get the histograms from only two narrow strips or slices from the discharging point at the bottom of the stack, the first one with slope of 60° — in the first quadrant — and the second one its mirrored image in third quadrant (it is like saying axes with azimuths of 30° and 330°, respectively, converging to the lower opening of the bin). For the initial image crop of each inclined strip, the overall image was rotated at the specified angles; the appropriate window was selected and cut, using the freeware computer package *Irfanview*. The thickness of each slice was 4.3% total stockpile height. The two strips of each stockpile were then rabatted

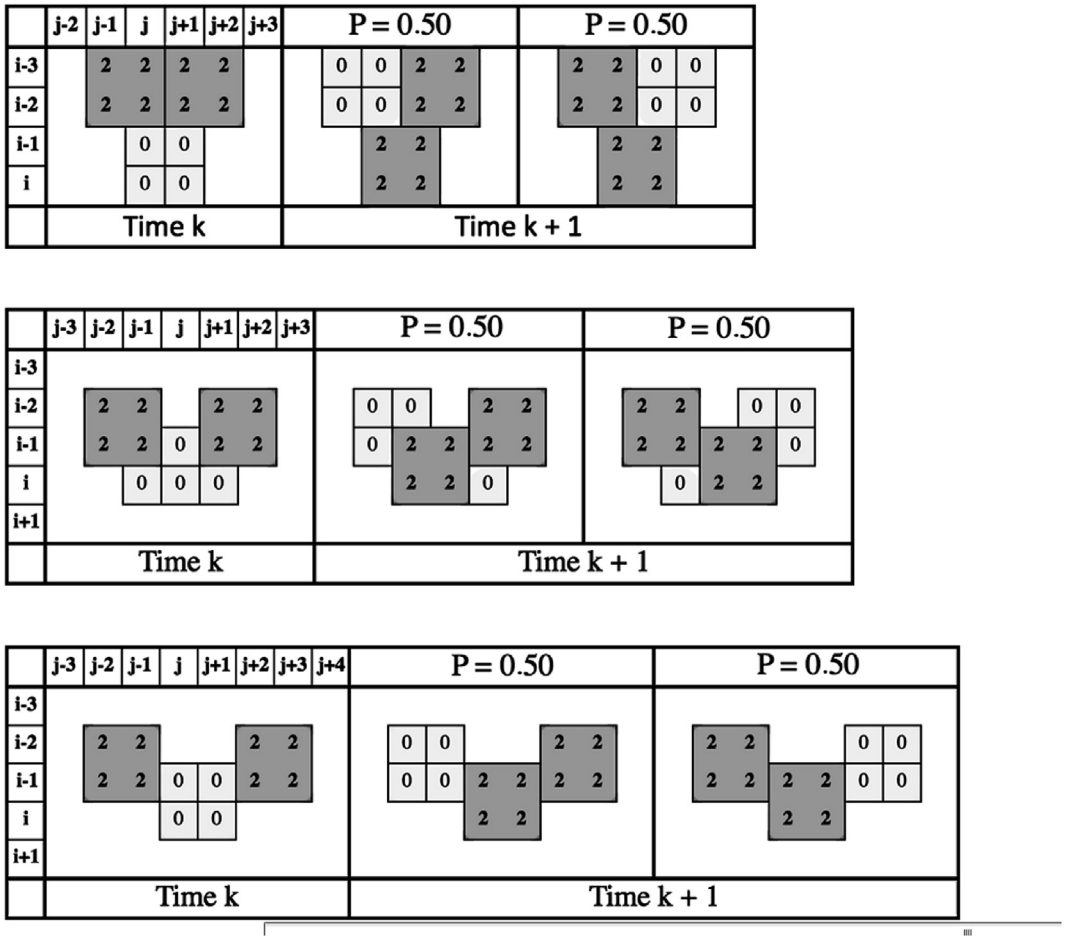

Fig. 6 – Probability rule for gravitational flow concerning particles of class P_2 (uppercase P in first the line is the probability of occurrence).

horizontally, forming a single strip representative of the spatial heterogeneity of the stockpile under analysis (after trimming of their ends).

The respective color histograms were extracted (with values from 0 to 255 —corresponding to the range from black to white, in the RGB color system), using an online histogram generator (https://www.dcode.fr/image-histogram). These histograms were checked using the corresponding tool from *Irfanview* as well.

Once in possession of the matrices of raw histograms: $H_{raw} = h(i, j)$, with i ranging from 0 to 255 (pixel value) and j ranging from 0.0 to 1.0 (relative frequency), the Cartesian ordered pairs were plotted, showing a clear mismatching in terms of brightness. As a matter of fact, even beforehand chromatic histograms were not expected to be the same. The actual experimental image (from the glass bin photos) encompasses a complex range of colors and shading, unlike the corresponding simulated image (which is rigorously had only a few colors formerly, for instance: white for interstitial voids, gray for the finer particles, and black for the coarser particles, in the case of binary mixing of the granular medium). In order to decrease this chromatic discrepancy, we chose to use simulated images generated by conventional image editing programs, instead of using the primitive pixel arrays, generated intrinsically by the simulation program.

The first idea that arises for the brightness equalization to improve the comparison of the pixel distribution is a constant pixel offset (it was found to be about $\gamma = 65$ later). However, this straightforward correction would lead to values above white, that is, values up to $255 + \gamma$. In order to avoid this contradiction, we have chosen to seek a monotonic correction function (including the factor γ) starting with the value 1.0, for the chromatic value 0 (black) up to zero, for the chromatic value 255 (white).

After several attempts, the following monotonic chromatic correction function (additive) was chosen:

$$y = x^{\alpha} \times \left(1 - x^{\beta}\right) \times \gamma \tag{4}$$

The parameters of this equation were determined tentatively by direct search, in order to minimize the quadratic sum of the deviations between the relative frequencies of the experimental data (from the quasi-two-dimensional glass bin) and the simulation data (from cellular automaton-based simulation). Correction function with inflections or periodic in its nature was avoided in order to prevent interference on the overall heterogeneity structure of each of the sample strips.

4. Results

Fig. 7 shows the stratification patterns formed in the physical model for a feed of 0.400 kg per each size range (total mass of 1.200 kg). The concentration of the finer particles near the stockpile axis is seen, while the coarser ones have concentrated on stockpile toe. The average mass flow rate at feed was 0.03 kg s^{-1}, and the thickness of successive layers achieved is consistent with the experiment results obtained by Grasselli and Herrmann [33].

After the first gravity reclaim of the stack live volume of approximately 0.600 kg of the granular solid, a new loading (new stacking or recharge) of this live volume was performed, with the same bulk solid of the first feed. The same stratification pattern occurs again, as seen in Fig. 7. During the initial stockpiling (Fig. 7), the composition of the recoverable (live or useful) volume is always of finer mean grain size than the feed, while the overall composition of the useful volume after first recharge actually corresponds to the stockpile feed (Fig. 8).

The cellular automaton-based model has reproduced the overall stratification features, as displayed in Fig. 9. Although it was not a persistent pattern neither the result appears to resemble the width of the layers obtained in the physical model, the segregation of the particles from the pile axis to the base was consistent enough to investigate quantitatively the material in the gravity flow discharge. The array had 60,971 particles of class P_1, which are depicted in light gray, 15,237 of class P_2 particles, in red, and 6766 particles of class P_3, in black.

Fig. 10 illustrates the raw chromatic histograms for the stockpile of Figs. 7 and 9. It clearly shows the mismatching of these histograms (curves 1 and 2) with higher brightness in the photograph referring to the experiment in the quasi-two-dimensional bin/pile.

The resulting parameters of the monotonic correction equation (Equation (4)) were: $\alpha = 5.4$; $\beta = 1.15$; $\gamma = 65$.

Chromatic corrections of slice associated to the simulated stockpile have implied abscissa changes. These changes would prevent the straightforward calculation of the deviations, because experimental and simulated (changed) data would fall in differing x abscissae (chromatic values). Therefore, it was necessary to interpolate the values of relative frequency (y) in the experimental data curve. After that, the relative frequencies (ordinates) in the experimental histogram (curve 1 in Fig. 10) could be properly compared with those corresponding to the simulated stockpile histogram (curve 3 in Fig. 10) over the corrected abscissae.

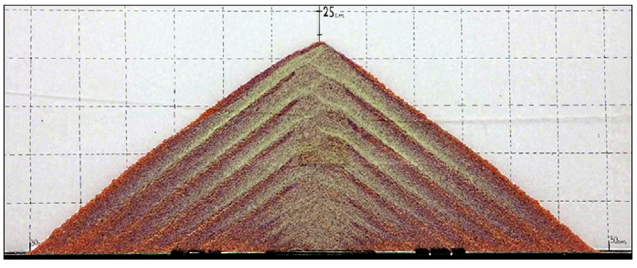

Fig. 7 – Quasi-two-dimensional stockpile after the first formation cycle, showing size segregation.

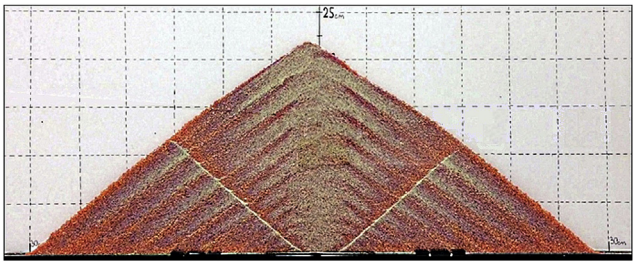

Fig. 8 – Quasi-two-dimensional stockpile built up again, after a first stockpiling and reclaim cycle.

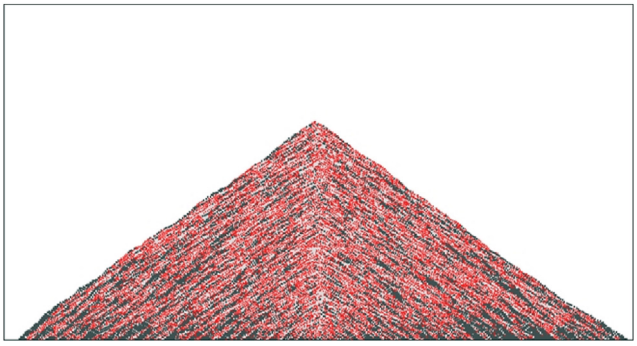

Fig. 9 – Cellular automaton-based simulation of a quasi-two-dimensional stockpile after the first formation cycle.

As a consequence of this brightness correction, curve 3 from Fig. 10 shows a discernible matching of the histograms of curve 1, showing now basically the same color heterogeneity. As a matter of fact, the cross-correlation of the raw pixel values was formerly equal to 0.02589. After the correction, the cross-correlation has increased to 0.87316.

In addition to the geostatistical techniques to measure the spatial heterogeneity of granular material stockpiles, mentioned briefly in a previous paragraph, analysis of the system's fractal dimensions can also be carried out with the same purpose. However, none of these approaches was attempted in the present work. In continuity to this line, a study of techniques of spatial heterogeneity characterization of granular systems will be carried out in the future, beyond the scope of the present article.

Similarly, to experimental feature (Fig. 8), the cellular automaton-based model restarts the stratification patterns from the new contours, when recharging the stack (Fig. 11).

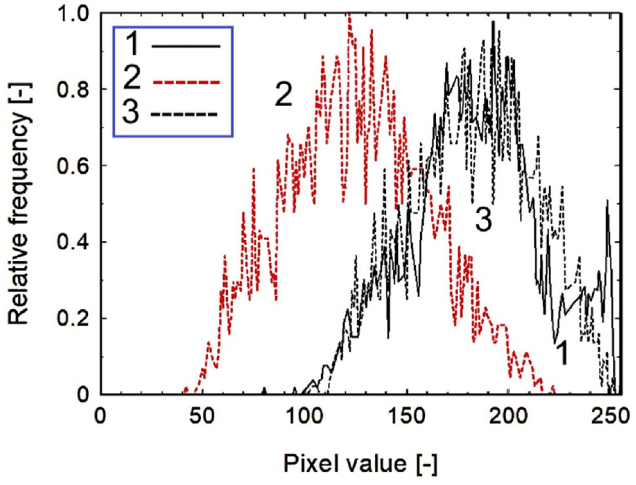

Fig. 10 – Chromatic histogram for experimental data (from Fig. 7 image), and raw and normalized histograms for cellular automaton-based simulation (from Fig. 9 image); curve 1 — experimental data (solid black line); curve 2 — simulated data before color correction (dashed red line), curve — simulated data after color correction (dashed black line).

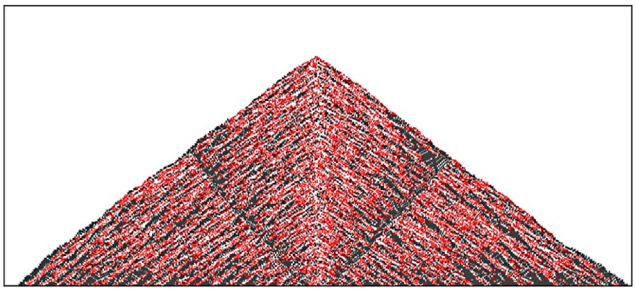

Fig. 11 – Cellular automaton-based simulation of a quasi-two-dimensional stockpile completely built up, after a first stockpiling and reclaim cycle.

4.1. *Granular flow behavior in reclaim operation*

Only the general features of the flow pattern obtained in the CA-based model are presented here. The concept of granular flow, developed by Janelid and Kvapil [13], describes well the flow behavior from these models. In Fig. 12, on the left, one observes the moment in which the initial flow ellipse reaches the surface of the pile, after drawing of about 2–5% of the live or useful volume. There is dilation of the porous space and larger gradients of vertical displacements in this region (Fig. 13, left). At the center of Fig. 12, after 50% of the useful volume having been drawn, one can see the material flowing by avalanches towards the axis of the stockpile, a hyperbolic surface forms in the flow outlines of the granular material, as can also be seen in Figs. 12 and 13 to the center. As it can see in Fig. 12 (on the right), at the end of the reclaim, the hyperbola degenerates into two straight lines with the slope equals to the angle of repose, delimiting the dead volume.

Gradients of horizontal and vertical displacements were made to see the evolution of granular flow. Plates 1, 2, and 3 from Fig. 13 display in darker shades the array regions where more movements occurred in the horizontal direction. Such sites are the stream surfaces where grain avalanches take place. In turn, in all the stages of the recovery, the movements to the left or right do cancel on the stockpile axis, leaving in lighter shade. In lower row of Fig. 13, Plate 4 (on the left), the isovalue lines of vertical displacements correspond to the various 'snapshots' of the flow ellipse, until it reaches the top of the stack. The vertical movements remain predominant in this region until the end of the discharge (Plates 5 and 6 from Fig. 13, center and right, respectively).

Another feature of particle size segregation during reclaiming flow is the preferential path of the coarser particles towards the axis of the stack. During avalanches, coarse particles segregate themselves over the finer particles. This phenomenon is known as kinematic sieving, free surface segregation, or even percolation according to Cizeau, Makse, and Stanley [36]. For this reason, the coarse particles first reach the axis of the pile, where there is the greatest vertical displacement gradient. Figure 14 illustrates this characteristic both in the corresponding physical model and cellular automaton-based model. A similar effect can be seen in works by Malakhov [37].

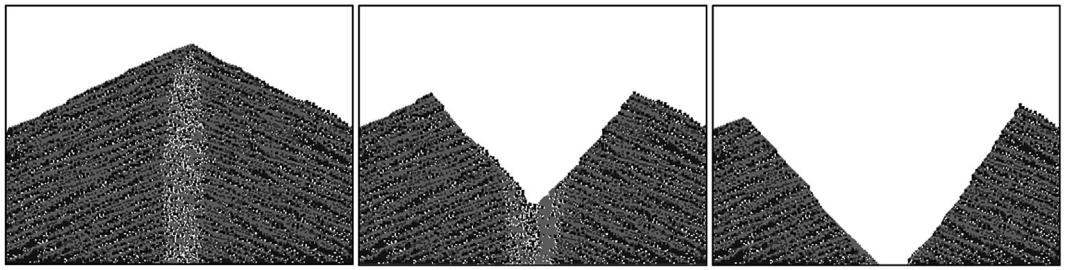

Fig. 12 – Stages of granular flow in reclaim: initial, intermediate, and final.

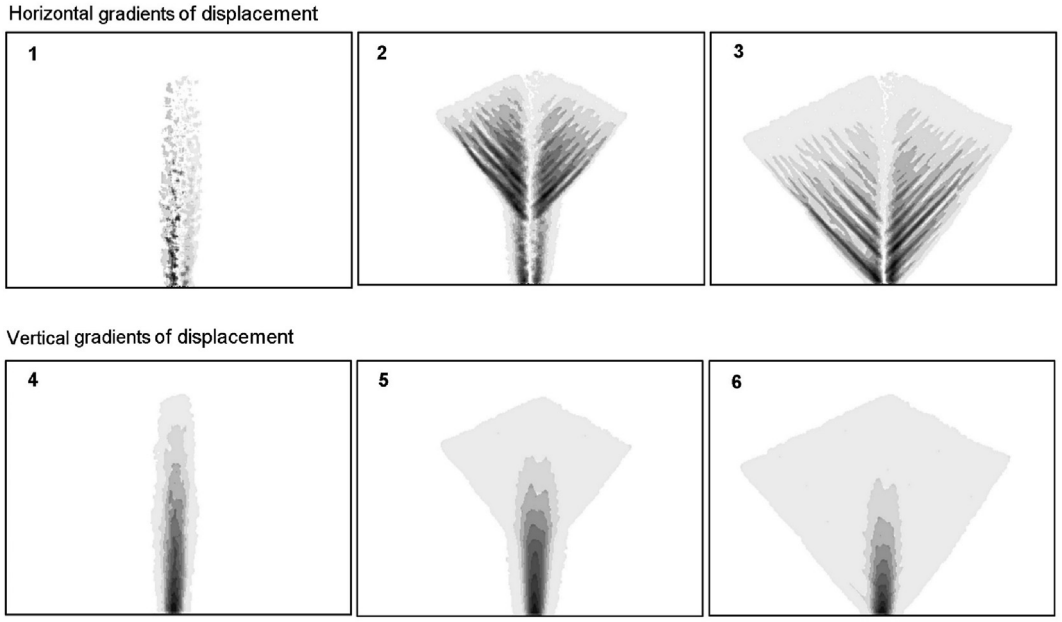

Fig. 13 – Displacement gradients: Plate 1 — initial horizontal gradient, Plate 2 —intermediate horizontal gradient; Plate 3 — final horizontal gradient; Plate 4 — initial vertical gradient; Plate 5 — intermediate vertical gradient; Plate 6 — final vertical gradient.

4.2. *Segregation effect during stockpile reclaim*

Samples taken during the reclaiming flow were normalized as percentages of the stockpile's live volume and plotted on the abscissa, analogously to a time scale, in Fig. 15. The corresponding ordinates are the mass percentages of each size range of the granular material (P_1, P_2 and P_3) during the reclaim. The points on the vertical axis — corresponding to 0% of live volume drawn —, refer to the feed composition (during stacking). This figure can be regarded as showing the evolution of the particle size proportions of granular material leaving the outlet slot as a function of the reclaiming time.

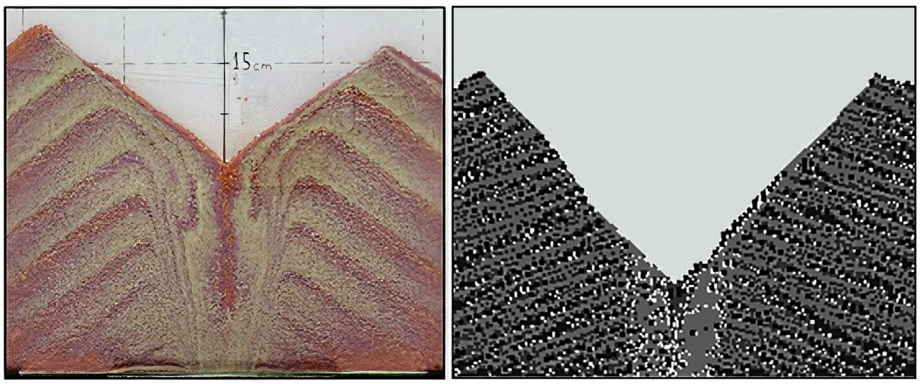

Fig. 14 – Segregation and preferential path in the physical model and mathematical (CA-based) model.

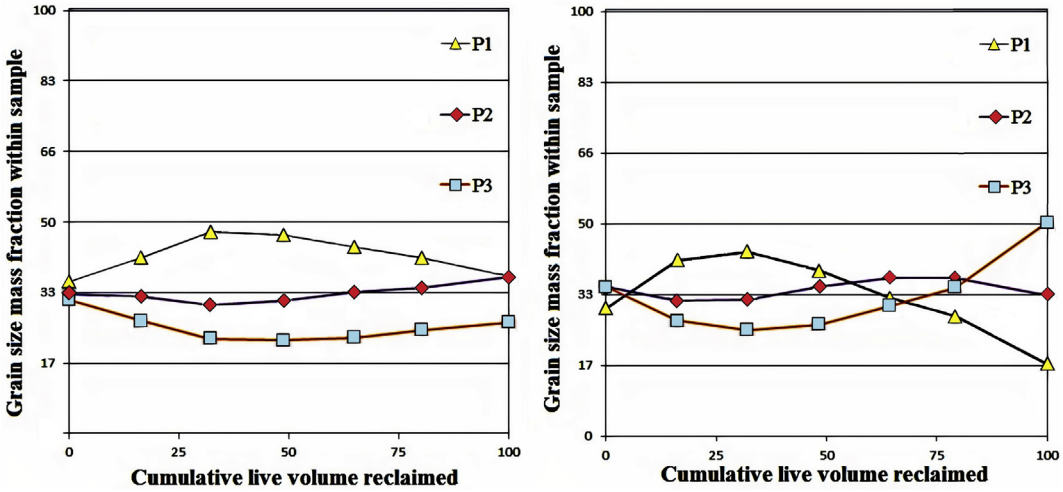

Fig. 15 – Reclaim experimental tests: left — evolution of particle size fractions during reclaim after first stockpiling; right — evolution of particle size fractions during reclaim after recharge.

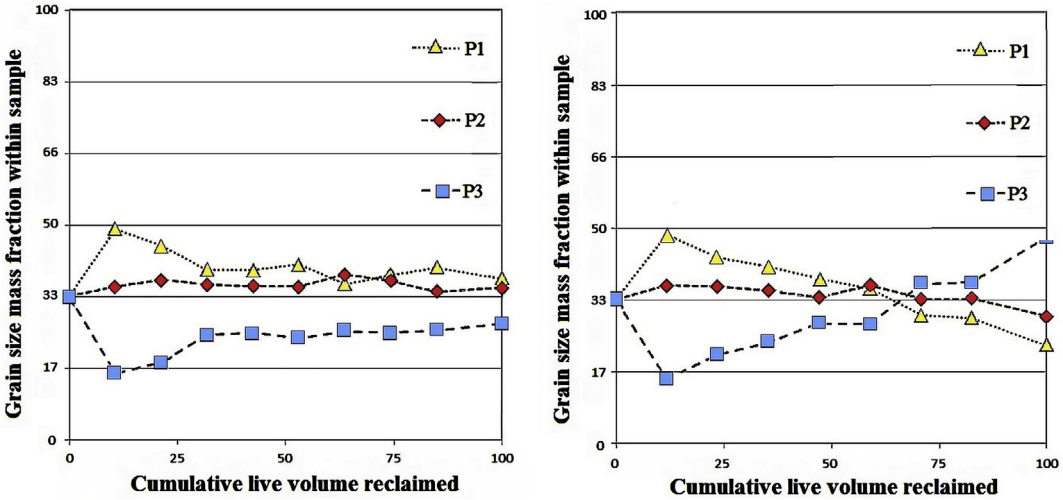

Fig. 16 – Reclaim simulation: left — evolution of particle size fractions during reclaim after first stockpiling; right — evolution of particle size fractions during reclaim after recharge.

Fig. 15 on the left shows downward concavity of the curve corresponding to the fine range material, and upward concavity for curve of coarser range material. The maximum of segregation, in a generic way, occurs when reclaiming amount was between 30% and 40% of the live volume. At the end of the curve, the material coming out from stockpile tends to return to the feed composition due to particle recovery by avalanches transverse to these stratified planes at the end of the stockpile discharge cycle.

On the other hand, Fig. 15 on the right displays results of a new reclaim cycle of a stockpile built up, after a first stockpiling and reclaim cycle (reclaim from an initial condition like that one displayed in Fig. 8).

In Fig. 15, on the right, predominantly fine material is inverted for a predominantly coarse one, after about 60% of the useful volume reclaimed. Concerning to the curves of the medium grain show slight inflection and oscillate between their initial value.

The cellular automaton-based model has reproduced the same behavior for the reclaim flow (Fig. 16). For the cellular automaton-based model, the particle curves also presented their respective concavities; however, the maximum segregation actually occurs before the first quarter of the live volume has drawn. And at the beginning of the last quarter of the live volume, the composition of the granular material at outlet slot already converges to initial composition, in the first reclaim cycle. In turn, in the second reclaim (after recharge) the inversion of the size composition also happens in a similar way to the case that occurs in the physical model (quasi-two-dimensional stack).

5. Conclusion

As far as this work's novelty is concerned, some of its features should be brought up. The high complexity of the behavior of non-cohesive particles being withdrawn from stockpiles, including self-organized criticality phenomena, makes it very difficult to quantitatively predict the stacking and the reclaim. Using the cellular automaton-based method (which uses simple rules to simulate complex systems), the contribution of the present paper is to enable a quick and expeditious tool for predictability of the behavior of densified granular systems, under gravitational flow, since information can be obtained from this proposed innovative model, with regard to particle size segregation, and the consequent spatial heterogeneity arising from the relative movement of particles during the stacking and reclaiming steps, in the normal operating cycle of industrial bulk handling operations.

As a matter of fact, the granular handling simulation here performed has allowed to predict variations in the characteristics of the granular material stored due to the particle size-segregation. The experiments performed in the quasi-two-dimensional physical model elucidate the behavior of granular materials in real and large-scale situations, according to their particle size distributions.

The cellular automaton-based model has been also successful in obtaining qualitative results for the expected stratification patterns. Likewise, it has obtained very satisfactory results in gravitational granular flow simulation. This programming technique has proved to be efficient for its ability to represent a dynamic situation with simple mathematical tools and computational resources.

The granular flow simulated by the AC-based model closely resembled the Janelid and Kvapil's granular flow ellipsoid [13] and indicates that the cellular automata simulation technique can be applied in the study of broken material flows inside underground mine employing sublevel caving and block caving methods, just to cite another example of application. This type of simulation can be very easily adapted for the forecasting of bulk solids behavior in bins and silos, often occurring in ore beneficiation plants and metallurgical complexes.

The model can still be easily implemented with modification in order to meet the case of mobile feed point, or, alternatively, in case of multiple discharge outlets. Its generalization to three dimensions is also possible. The simplest model of this generalization to a conic pile (which is a solid of revolution) could be done by applying the Pappus-Guldinus theorem. Indeed, it should be born in mind that the live or useful volume of a two-dimensional stockpile differs substantially from that corresponding to a three-dimensional conic stockpile, as calculated by the application of said theorem (because it is an axisymmetric system).

Declaration of Competing Interest

The authors declare that they have no known competing financial interests or personal relationships that could have appeared to influence the work reported in this paper.

Acknowledgement

The authors thank to Brazilian Council for Technological and Scientific Development (CNPq), Foundation for Research Support of the State of Minas Gerais (FAPEMIG), and Brazilian Federal Agency for Support and Coordination for the Improvement of Higher Education Personnel (CAPES) for their financial support.

REFERENCES

[1] Herrmann HJ, Luding S. Modeling granular media on the computer. Continuum Mech Therm 1998;10:189–231. https://doi.org/10.1007/s001610050089.
[2] Herrmann HJ. Granular matter. Phys A Stat Mech Its Appl 2002;313:188–210. https://doi.org/10.1016/S0378-4371(02)01037-3.
[3] Romanowski A, Grudzien K, Williams RA. Analysis and interpretation of hopper flow behaviour using electrical capacitance tomography. Part Part Syst Char 2006;23:297–305. https://doi.org/10.1002/ppsc.200601060.
[4] Larsson S, Gustafsson G, Oudich A, Jonsén P, Häggblad HÅ. Experimental methodology for study of granular material flow using digital speckle photography. Chem Eng Sci 2016;155:524–36. https://doi.org/10.1016/J.CES.2016.09.010.
[5] Tucci G, Gebbia A, Conti A, Fiorini L, Lubello C. Monitoring and computation of the volumes of stockpiles of bulk material by means of UAV photogrammetric surveying. Rem Sens 2019;11:1471. https://doi.org/10.3390/RS11121471.
[6] Luz JAM, Peres AEC. Cálculo de Volume Útil de Pilhas de Granéis pelo Método de Monte Carlo Simples. An. do III Encontro do Hemisfério Sul sobre Tecnol. Miner., São Lourenço: ABM; 1992. p. 604–23.
[7] Ai J. Particle scale and bulk scale investigation of granular piles and silos. 2010.
[8] Beakawi Al-Hashemi HM, Baghabra Al-Amoudi OS. A review on the angle of repose of granular materials. Powder Technol 2018;330:397–417. https://doi.org/10.1016/J.POWTEC.2018.02.003.
[9] Benito JG, Ippolito I, Vidales AM. Novel aspects on the segregation in quasi 2D piles. Powder Technol 2013;234:123–31. https://doi.org/10.1016/J.POWTEC.2012.09.043.
[10] Rodríguez D, Benito JG, Ippolito I, Hulin J-P, Vidales AM, Uñac RO. Dynamical effects in the segregation of granular mixtures in quasi 2D piles. Powder Technol 2015;269:101–9. https://doi.org/10.1016/J.POWTEC.2014.09.001.
[11] Larcher M, Jenkins JT. The influence of granular segregation on gravity-driven particle-fluid flows. Adv Water Resour 2019;129:365–72. https://doi.org/10.1016/J.ADVWATRES.2017.07.025.
[12] Liao CC, Hsiau SS, Wen SF. Effect of adding a small amount of liquid on density-induced wet granular segregation in a rotating drum. Adv Powder Technol 2016;27:1265–71. https://doi.org/10.1016/J.APT.2016.04.015.
[13] Janelid I, Kvapil R. Sublevel caving. Int J Rock Mech Min Sci Geomech Abstr 1966;3:129–32. https://doi.org/10.1016/0148-9062(66)90004-0.
[14] Brady BHG, Brown ET. Rock Mechanics for underground mining. ed. Netherlands: Springer; 2006. https://doi.org/10.1007/978-1-4020-2116-9.
[15] Zhao H-T, Yang S, Chen X-X. Cellular automata model for urban road traffic flow considering pedestrian crossing

street. Phys A Stat Mech Its Appl 2016;462:1301–13. https://doi.org/10.1016/J.PHYSA.2016.06.146.
[16] Regragui Y, Moussa N. A cellular automata model for urban traffic with multiple roundabouts. Chin J Phys 2018;56:1273–85. https://doi.org/10.1016/j.cjph.2018.02.010.
[17] Tang TQ, Rui YX, Zhang J, Shang HY. A cellular automation model accounting for bicycle's group behavior. Phys A Stat Mech Its Appl 2018;492:1782–97. https://doi.org/10.1016/J.PHYSA.2017.11.097.
[18] Georgoudas IG, Sirakoulis GC, Scordilis EM, Andreadis I. A cellular automaton simulation tool for modelling seismicity in the region of Xanthi. Environ Model Software 2007;22:1455–64. https://doi.org/10.1016/J.ENVSOFT.2006.06.015.
[19] di Caprio D, Stafiej J, Luciano G, Arurault L. 3D cellular automata simulations of intra and intergranular corrosion. Corrosion Sci 2016;112:438–50. https://doi.org/10.1016/J.CORSCI.2016.07.028.
[20] Gurikov P, Kolnoochenko A, Golubchikov M, Menshutina N, Smirnova I. A synchronous cellular automaton model of mass transport in porous media. Comput Chem Eng 2016;84:446–57. https://doi.org/10.1016/J.COMPCHEMENG.2015.10.001.
[21] Ogawa J, Natsume Y. Three-dimensional large-scale grain growth simulation using a cellular automaton model. Comput Mater Sci 2021;199:110729. https://doi.org/10.1016/J.COMMATSCI.2021.110729.
[22] Kim MS, Lee SH, Jung JG, Eah K. Prediction of grain structure in direct-chill cast Al–Zn–Mg–Cu billets using cellular automaton-finite element method. Prog Nat Sci Mater Int 2021;31:434–41. https://doi.org/10.1016/J.PNSC.2021.05.003.
[23] Wang D, Bai Y, Xue C, Wang Q, Yu H, Yan Z. Grain evolution simulation of ceramic tool material in spark plasma sintering process based on an improved cellular automata model. Ceram Int 2021;47:13669–77. https://doi.org/10.1016/J.CERAMINT.2021.01.228.
[24] Xiao X, Shao S-H, Chou K-C. A probability cellular automaton model for hepatitis B viral infections. Biochem Biophys Res Commun 2006;342:605–10. https://doi.org/10.1016/J.BBRC.2006.01.166.
[25] Wan C, Liu Y, Tu X-M, Zhang Y-Y, Xu J-M, Lin D-D, et al. A cellular automaton model of Schistosoma japonicum infection. Acta Trop 2013;126:256–64. https://doi.org/10.1016/J.ACTATROPICA.2013.02.012.
[26] Precharattana M, Triampo W. Modeling dynamics of HIV infected cells using stochastic cellular automaton. Phys A Stat Mech Its Appl 2014;407:303–11. https://doi.org/10.1016/J.PHYSA.2014.04.007.
[27] Cavalcante ALB, Borges LP de F, Lemos MA da C, Farias MM de, Carvalho HS. Modelling the spread of covid-19 in the capital of Brazil using numerical solution and cellular automata. Comput Biol Chem 2021;94:107554. https://doi.org/10.1016/J.COMPBIOLCHEM.2021.107554.
[28] Jithesh PK. A model based on cellular automata for investigating the impact of lockdown, migration and vaccination on COVID-19 dynamics. Comput Methods Progr Biomed 2021;211:106402. https://doi.org/10.1016/J.CMPB.2021.106402.
[29] Podolski P, Nguyen HS. Cellular automata in covid-19 prediction. Procedia Comput Sci 2021;192:3370–9. https://doi.org/10.1016/J.PROCS.2021.09.110.
[30] Alonso JJ, Hovi J-P, Herrmann HJ. Lattice model for the calculation of the angle of repose from microscopic grain properties. Phys Rev E 1998;58:672–80. https://doi.org/10.1103/PhysRevE.58.672.
[31] Silva JM da. Estudo do fluxo de material fragmentado na mineração subterrânea, com o uso de modelos físicos. Universidade Federal de Minas Gerais; 2005.
[32] Fan Y, Boukerkour Y, Blanc T, Umbanhowar PB, Ottino JM, Lueptow RM. Stratification, segregation and mixing of granular materials in quasi-2D bounded heaps. Phys Rev E 2012;86:1–13. https://doi.org/10.1103/PhysRevE.86.051305.
[33] Grasselli Y, Herrmann HJ. Experimental study of granular stratification. Granul Matter 1998;1:43–7. https://doi.org/10.1007/PL00010909.
[34] Box GEP, Muller ME. A note on the generation of random normal deviates. Ann Math Stat 1958;29:610–1. https://doi.org/10.1214/aoms/1177706645.
[35] Kozicki J, Tejchman J. Simulations of flow patterns in silos with a cellular automaton: Part 1. TASK Q Sci Bull Acad Comput Cent Gdansk 2005;9:81–102.
[36] Cizeau P, Makse HA, Stanley HE. Mechanisms of granular spontaneous stratification and segregation in two-dimensional silos. Phys Rev E 1999;59:4408–21. https://doi.org/10.1103/PhysRevE.59.4408.
[37] Shevyakov LD. Mining of mineral deposits; a textbook [translated from the Russian by V. Schiffer]. Moscow: Foreign Languages Pub. House; 1963.